Migraine inhibitor olcegepant reduces weight loss and IL-6 release in SARS-CoV-2 infected older mice with neurological signs

Shafaqat M. Rahman[1,&], David W. Buchholz[2,&], Brian Imbiakha[2,&], Mason.C. Jager[3], Justin Leach[1], Raven.M. Osborn[1], Ann O. Birmingham[1], Stephen Dewhurst[1], Hector C. Aguilar[2,*], and Anne E. Luebke[1,*]

[1]University of Rochester Medical Center, Departments of Biomedical Engineering, Neuroscience, Microbiology and Immunology, Rochester, NY, USA;

[2] Cornell University, Department of Microbiology and Immunology, College of Veterinary Medicine, Ithaca, NY, USA.

[3] Cornell University, Department of Population Medicine, College of Veterinary Medicine, Ithaca, NY, USA.

[&]Contributed equally

*Send correspondence to:

Anne E. Luebke (aluebke@ur.rochester.edu)

or

Hector C. Aguilar (haguilar@cornell.edu)

Running title: Migraine inhibitor helps older COVID mice

Abstract

COVID-19 can result in neurological symptoms such as fever, headache, dizziness, and nausea. However, neurological signs of SARS-CoV-2 infection have been hardly assessed in mouse models. Here, we infected two commonly used wildtype mice lines (C57BL/6 and 129S) with mouse-adapted SARS-CoV-2 and demonstrated neurological signs including motion-related dizziness. We then evaluated whether the Calcitonin Gene-Related Peptide (CGRP) receptor antagonist, olcegepant, used in migraine treatment could mitigate acute neuroinflammatory and neurological responses to SARS-COV-2 infection. We infected wildtype C57BL/6J and 129/SvEv mice, and a 129 αCGRP-null mouse line with a mouse-adapted SARS-CoV-2 virus, and evaluated the effect of CGRP receptor antagonism on the outcome of that infection. First, we determined that CGRP receptor antagonism provided protection from permanent weight loss in older (>12 m) C57BL/6J and 129 SvEv mice. We also observed acute fever and motion-induced dizziness in all older mice, regardless of treatment. However, in both wildtype mouse lines, CGRP antagonism reduced acute interleukin 6 (IL-6) levels by half, with virtually no IL-6 release in mice lacking αCGRP. These findings suggest that migraine inhibitors such as those blocking CGRP signaling protect against acute IL-6 release and subsequent inflammatory events after SARS-CoV-2 infection, which may have repercussions for related pandemic and/or endemic coronaviruses.

44 **Importance**

45 COVID-19 can cause neurological symptoms such as fever, headache, dizziness, and nausea.
46 However, such neurological symptoms of SARS-CoV-2 infection have been hardly assessed in
47 mouse models. Here, we first infected two commonly used wildtype mice lines (C57BL/6 and
48 129S) with mouse-adapted SARS-CoV-2 and demonstrated neurological signs including
49 motion-related dizziness. Further, we showed that migraine treatment drug olcegepant could
50 reduce long-term weight loss and IL-6 release associated with SARS-CoV-2 infection. These
51 findings suggest that a migraine blocker can be protective for at least some acute SARS-CoV-2
52 infection signs and raise the possibility that it may also impact long-term outcomes of infection.
53

Introduction

Coronavirus disease (COVID-19) caused by severe acute respiratory syndrome CoV-2 (SARS-CoV-2) has caused a 4-year world pandemic (1). Headache, nausea, and dizziness are common neurological manifestations of COVID-19 infection (2-4), and in COVID-19 patient's headache severity has been correlated with IL-6 levels (5). It is accepted that migraine involves the neuropeptide calcitonin gene-related peptide (CGRP). CGRP is up regulated during migraine attacks (6, 7), infusion of CGRP can induce migraine (7), and antibodies that block CGRP or its receptor can effectively treat most migraines (8, 9). This supports the testing of migraine inhibitors such as CGRP receptor antagonists, e.g. olcegepant, as a way to mitigate the neuroimmune consequences of SARS-CoV-2 infection (10).

While CGRP has pleotropic effects on the immune system, CGRP release occurs as a result of SARS-CoV-2 activation of the transient receptor potential (TRP) channels; and is implicated in COVID-19 neurological symptoms such as fever, headache, dizziness, nausea pain, and the subsequent release of interleukin 6 (IL-6) (11-13). IL-6 is an important mediator of inflammation that is often elevated in severe COVID-19 infection and may be involved in the hyperimmune response cascade (cytokine storm) and the polarization of T-cell responses (14, 15). However, there have been no studies on animal models investigating dizziness and fever after SARS-CoV-2 infection (16) .

Studies have shown that both SARS-CoV-1 and SARS-CoV-2 enter the body by binding to the angiotensin-converting enzyme 2 (ACE2) cell receptor (17, 18). However, due to sequence and structural differences between mouse ACE2 and human ACE2, human SARS coronaviruses exhibit a species-restricted tropism and are inefficient at infecting wild-type mice. To overcome this obstacle, the Baric laboratory selected a clinical SARS-CoV-2/USA-WA1 variant that gained the ability to bind to the murine ACE2 receptor after serial passaging in mice, to generate virus MA10-SARS-CoV-2 (19, 20).

We used MA10-SARS-CoV-2 to assess both neurological symptoms of fever and dizziness/nausea in mouse models after infection. As a readout of the nausea-like state present after SARS-CoV-2 infection, we examined hypothermic responses to provocative motion, as we have previously used to assess migraine nausea pain (21) and others have used to assess motion-sensitivity in transgenic mouse models (22). Studies have demonstrated that provocative motion causes robust and prominent hypothermic responses in rats, humans, house musk shrews, and mice. Such decreases in body temperature can represent a biomarker of a nausea-like state in laboratory animals as: i) temperature changes are provoked both by motion and by chemical emetic stimuli, ii) differential pharmacological sensitivity of these responses mirrors sensitivity in humans, iii) motion-induced hypothermia *precedes* emetic (vomiting) episodes, and iv) there is a clear parallel in hypothermic responses between animals and humans in underlying physiological mechanism - cutaneous vasodilatation that favors heat loss (22-26). In the nausea/dizziness assay after provocative motion there is a decrease in head temperature and an increase in tail temperature. We have shown that in wildtype C57BL/6J mice injection of CGRP prolongs the head temperature response and blunts the transient tail temperature increase, whereas a CGRP-receptor antagonist can reverse these CGRP-induced changes (21, 27, 28). Therefore, we investigated if a MA10-SARS-CoV-2 viral infection would show similar acute dizziness/nausea responses as CGRP injection, and if antagonizing CGRP signaling could reduce these dizziness/nausea responses and/or other signs of SARS-CoV-2 infection.

102 **Results**

103 **MA-10 SARS-CoV-2 infection induces a fever-like state and disrupts**
104 **thermoregulation to provocative motion.** We measured baseline head temperatures in 18
105 month-old male C57BL/6J, 129SvEv, and 129 αCGRP-null groups of mice during pretesting and
106 3 days post-infection (dpi) with 10^5 pfu of MA-10 SARS-CoV-2 virus (**Fig. 2A & B**). Our results
107 showed a higher head temperature at 3 dpi, indicating a fever in all mice, regardless of strain
108 and olcegepant pretreatment (**Fig. 2B**).

109 We also measured motion-induced thermoregulation and weight changes in 18 month-
110 old male C57BL/6J, 129SvEv, and 129 αCGRP-null groups of mice at 3 dpi with 10^5 pfu of MA-
111 10 SARS-CoV-2 virus (**Fig. 3A**). Motion-induced thermoregulation was pre-tested in each
112 mouse 5-7 days prior to the infection. During the pre-test, we observed transient tail vasodilation
113 in response to provocative, nauseating stimuli (**Fig. 3B, C, D**). The assay involved a 5-minute
114 baseline recording, a 20-minute rotation period (75 rpm, 1 cm orbital displacement), and a 20-
115 minute recovery/observation period (as shown in **Figs. 1B and 3A**). Tail temperature profiles
116 also indicated a fever-like state after infection with MA-10 SARS-CoV-2, with higher tail
117 temperatures at all time points during the 3 dpi test than during the pretest (**Fig. 3B, C, D**). We
118 computed a shift in the Δ tail vasodilations by subtracting the magnitude of Δ tail vasodilations at
119 3 dpi from an animal's pretest Δ tail vasodilation. With the exception of infected αCGRP-null
120 mice, we observed a decrease in the magnitude of tail vasodilations in infected mice compared
121 to their pretest, as indicated by a negative change in the Δ tail vasodilation, a sign of change in
122 the level of severe dizziness.

123 Typically, a twenty-minute provocative rotation in mice causes observable hypothermia,
124 and an additional 20-minute recovery period is needed for the mice to recover to their baseline
125 head temperature. Interestingly, we observed that viral infection delayed this recovery period, as
126 seen in our raw data (**Fig. 3 E, F, G**). Using a second-order polynomial fit ($B_0 + B_1X + B_2X^2$), we
127 estimated the time required for the mice to recover back to their baseline head temperature by

128 interpolating a curve fit to t = 50 minutes (**Fig. 3H).** We then computed a Δ head recovery by
129 subtracting the recovery period at 3 dpi from the pretest, where a positive Δ head recovery
130 indicated a longer recovery period due to the infection. In all infected males, regardless of
131 olcegepant treatment or strain, we observed a longer recovery period at 3 dpi ($p < 0.0001$). No
132 protective effects were seen by olcegepant in head temperature recovery for either strain (**Fig.**
133 **3H**).

134

135 **Olcegepant blockage or developmental loss of CGRP receptor leads to reduced IL-6**
136 **production in response to MA-10 infection.** Interestingly, SARS-CoV-2 infected 129/SvEv
137 mice treated with olcegepant pellets had lower interleukin 6 (IL-6) concentrations in their
138 bronchoalveolar lavage (BAL) as compared to mice treated with placebo ($p < 0.05$) (**Fig. 4B**).
139 Congruently, the lower IL-6 concentrations in olcegepant-treated mice were similar to the IL-6
140 concentrations measured in the αCGRP-null (-/-) mice (**Fig. 4B**), which is consistent with the
141 relationship between CGRP and IL-6 levels in migraines (29). In C57BL/6J mice, similar trends
142 in olcegepant effects in reducing IL-6 post-infection were observed, but did not reach statistical
143 significance (**Fig. 4A**).

144

145 **Older mice treated with olcegepant recovered from the initial weight loss by 7 dpi.**
146 Interestingly, when 18-month-old C57 or 129S mice were infected with MA-10, those pretreated
147 with olcegepant pellets showed a faster recovery to baseline weight compared to mice that
148 received placebo pellets. This effect was observed in both female and male C57BL/6J mice
149 (**Fig. 5A**), as well as in older female and male 129SvEv mice (**Fig. 5B**). Notably, 129S αCGRP
150 (-/-) null mice of either sex experienced similar trends as 129S WT mice given olcegepant (**Fig.**
151 **5E**). Further, older infected mice exhibited lower core temperatures compared to the uninfected
152 groups. However, olcegepant had no distinguishable effect on core temperatures regardless of

153 age or strain (**Fig. 5 B, D, F**). In addition, MA-10 infection did not significantly impact O_2%
154 saturation levels in mice regardless of age, sex, or strain. However, αCGRP-null mice exhibited
155 lower weight loss trends following virus infection that did WT mice, suggesting that the αCGRP-
156 null mice had reduced severe signs of disease.

157 Histological analysis of lung tissue revealed no significant differences in the number of
158 SARS-CoV-2 infected cells in the lungs of C57BL/6J or 129S WT mice at 3 dpi (**Fig. 6 A & B**).
159 However, olcegepant-treated mice and αCGRP-null mice showed reduced staining for SARS-
160 CoV-2 when compared to placebo-treated mice, and this observation correlated with the
161 reduced IL-6 levels. **Fig. 6 C&D** shows SARS-CoV-2 staining (scale = 100 μm) of C57BL/6J (**C**)
162 and 129S (**D**) lung tissues.

163

164

165 **Discussion**

166 Neurological signs of SARS-CoV-2 infection have been hardly assessed in mouse
167 models. Here, we infected two commonly used wildtype mice lines (C57BL/6 and 129S) with
168 mouse-adapted SARS-CoV-2 strain MA-10. Importantly, we demonstrated for the first time the
169 neurological signs of motion-related dizziness, with fever and dizziness/nausea-like state
170 elicited by SARS-CoV-2 MA-10 at 3 dpi. These results are consistent with associated fever and
171 vestibular symptoms observed in COVID patients (30, 31). Early in the pandemic, there was a
172 controversy as to whether CGRP plasma levels were increased or decreased in COVID-19
173 disease (32, 33). However, a recent study with a relatively greater number of patients showed
174 that elevated CGRP plasma levels are correlated with increased disease severity in hospitalized
175 COVID-19 patients (34). Notably, in our study the migraine drug olcegepant (small molecule
176 CGRP receptor antagonist) reduced weight loss post-infection as well as IL-6 release at three
177 days post-infection (3 dpi) in two distinct wildtype mouse strains (C57B6 and 129S), even in the
178 absence of an effect on the level of dizziness in the infected animals.

179 A few studies have investigated CGRP antagonism on individuals infected with SARS-
180 CoV-2. In one study (37), no deleterious effects of CGRP antagonism were found, and no
181 differences in symptom severity were found between CGRP antagonisms to other treatment
182 modalities in migraine subjects. However, in this study, patients were not stratified by age. We
183 are the first to show that inhibiting CGRP signaling – via olcegepant and in the αCGRP-null (-/-)
184 mice - protects against weight loss and reduces IL-6 release *in older mice*. COVID-19
185 symptoms are more severe and mortality rates are higher in aged human patients, adding
186 significance to our results. Further, two relatively recent case studies showed that increased
187 headaches after SARS-CoV-2 infection can be treated with CGRP monoclonal antibodies (38,
188 39). Our study suggests that olcegepant or other CGRP treatments may be further explored
189 particularly to treat headaches or migraine in aged individuals and/or those with high IL-6 levels
190 upon COVID-19 infection.

In conclusion, in addition to the acute neurological effects studied here, antagonizing CGRP signaling may be an off-the-shelf therapeutic against long COVID, as long COVID patients also show higher IL-6 plasma levels (40). As long COVID has been demonstrated in mouse models (41), future plans include investigating if antagonizing CGRP signaling in preclinical models can mitigate associated neurological symptoms of long COVID (42). Further, the results of our study may have implications for other coronaviral diseases, such as those caused by future pandemic (SARS-CoV-1, MERS-CoV, etc…) or endemic coronaviruses.

200 **Materials and Methods**

201 **Animals.** A total of 180 mice (120 M/60F) were used in these studies, either 129SvEv (Taconic
202 129SVE) or C57BL/6J (JAX 0664) or αCGRP (-/-) null mice on a 129SvEv background. Prior to
203 SARS-CoV-2 infection, mice were bred and housed under a 12 to 12 day/night cycle at the
204 University of Rochester 's Vivarium under the care of the University of Rochester's Veterinary
205 Services personnel. Mice were implanted with transponder chips (Backagin Microchip FDX-B
206 ISO 11784/11785) to allow for blinded identification; and when relevant, implanted with pellets
207 containing placebo or olcegepant (BIBN4096, Tocris; 2 mg/kg/day/SQ; Innovative Research of
208 America, Inc.). After pretesting was performed, mice were transferred to Cornell's ABSL3
209 facility, and acclimated prior to virus infection and testing. All animal procedures were approved
210 both by the University of Rochester's and Cornell University's IACUC committees and
211 performed in accordance with NIH standards.

212

213 **Virus propagation.** Vero-E6 cells (obtained through BEI resources, NIAID, NIH, NR-53726)
214 were cultured in Eagle's Minimum Essential Medium (ATCC, #30-2003) supplemented with 10%
215 (vol/vol) fetal bovine serum (FBS) (Gibco, CA) and 1% penicillin-streptomycin (Pen-Strep, Life
216 Technologies) at 37°C in a 5% (vol/vol) CO_2 atmosphere. Viral stocks of mouse-adapted SARS-
217 CoV-2 (MA10) (obtained from the laboratory Dr. Ralph Baric) were propagated in Vero-E6 cells
218 in 2% (vol/vol) FBS and 1% penicillin-streptomycin at 37°C at a multiplicity of infection (MOI) of
219 0.1. Viral stock titers were determined by $TCID_{50}$ analysis. Viral propagation involving live
220 SARS-CoV-2 was conducted in Biosafety level 3 (BSL3) facilities both at the University of
221 Rochester and at Cornell University.

222

223 **Animal Biosafety level 3 (ABSL3) facility and viral inoculations.** Mice were anesthetized
224 using isofluorane and subsequently intranasally infected with MA-10 SARS-CoV-2. For infection

225 with live virus, drops of the pre-characterized viral stock were administered into the rostral
226 meatus of the nose, with a total volume of 50 µL per mouse. Daily monitoring and weighing of
227 the mice were conducted until they reached a predetermined humane endpoint of 20% weight
228 loss from their starting weight and/or severe clinical signs, at which point animals were
229 humanely euthanized. Mouse studies were conducted in a BSL-3 laboratory and in accordance
230 with protocols approved by the Institutional Animal Care and Use Committee at Cornell
231 University (IACUC mouse protocol # 2017-0108 and BSL3 IBC # MUA-16371-1).
232

233 **Motion-Induced Thermoregulation Testing.** Tu et al. first noticed thermoregulatory
234 changes in the temperatures of the heads, bodies, and tails of mice, in response to
235 provocative motion (22). We therefore adapted their protocol for the present study. Head
236 and tail temperatures of C57B6/J mice were measured for a total of 45 minutes using a FLIR
237 E60 IR camera (model: E64501), as depicted in **Fig. 1A**. This camera was connected to a tripod
238 and positioned approximately 43 cm above an open, plexiglass box (mouse box) used to house
239 an individual mouse during testing. Both the tripod and mouse box were securely attached to
240 the shaker's base. Briefly, baseline measurements were recorded for five minutes prior to the
241 provocative motion (-5 to 0 mins). The provocative motion was an orbital rotation (75 rpm, 2-cm
242 orbital displacement), and mice were video-recorded for 20 minutes (0 to 20 mins). After 20
243 minutes, the provocative motion was turned off, and mice were video recorded for an additional
244 20 minutes to measure recovery to baseline (20 to 40 mins) as schematized in Figs. 1A and 2.
245 Head and tail temperatures were measured after data retrieval using the software FLIR Tools+.
246 Tail and head temperatures were measured within predefined field of views: square region (3x3
247 mm) for tail, and circular region (10x10 mm) for head. Tail measurements occurred 2 cm from
248 the base of the tail and head measurements occurred at the center of the head image, in
249 between the mouse's ears. Infrared imaging data was collected every minute during baseline
250 measurements, and every 2 minutes during and after the provocative motion. We quantified

251 thermoregulatory changes to provocative motion by comparing changes in tail vasodilatations,
252 and we approximated the magnitude of the head hypothermia based on second order curve fit
253 estimates. Transient increases in the tail temperature of the mouse to provocative motion are
254 referred to as Δ *tail vasodilatations* (^{o}C), and were computed by subtracting the tail temperature
255 at time t = 0 minutes (rotation ON) from the max tail temperature measured during the first 10
256 mins of the rotation ($0 \leq t \leq 10$).

257

258 **Pulse Oximetry.** A mouse Stat Jr X (Kent Scientific) was used to measure oxygen saturation
259 (O2%) of mice (see Fig. 1B). The O_2 sensor was applied to the rear leg, and data were recorded
260 following readout stabilization, defined as an unchanging recording over 5 seconds.

261

262 **BAL harvest and tissue processing.** Mice were euthanized with CO_2, and bronco-alveolar
263 lavage BAL fluid was removed from the lung; animals then underwent laparotomy and
264 sternotomy with subsequent left and right ventricular cardiac perfusion with 20 mL total of PBS.
265 Lungs were treated with 4% paraformaldehyde/PBS (volume/volume) for a minimum of 72 hours
266 to ensure full viral inactivation. Tissues were taken out of the BSL3 facility and underwent
267 dehydration with ethanol and were later embedded in paraffin blocks for histological analysis.

268

269 **Histopathology.** For histological examination, mouse lungs were collected directly after
270 euthanasia and placed in 10% neutral buffered formalin for 72 h, after which tissues were
271 embedded in paraffin. Four-micrometer tissue sections were stained with hematoxylin for
272 analysis. Immunohistochemistry and digital image analysis for SARS-CoV-2 nucleocapsid was
273 performed as previously described (43). Briefly, 4 μm tissue sections were labeled with a rabbit
274 IgG monoclonal antibody against SARS-CoV-2 nucleocapsid protein (GeneTex; GTX635679) at

275 a 1:5,000 dilution and processed using a Leica Bond Max automated IHC Stainer. Digital image
276 analysis was performed using QuPath software v.0.2.3 (43-46).

277

278 **Imaging.** Histological specimens were visualized using a Zeiss Axioplan 2 microscope.
279 Immunohistochemistry (IHC) and hematoxylin and eosin (HE) stained slides for each specimen
280 were photographed in sequential order. In Adobe Photoshop, all images were sized with a
281 2080x2080 pixel frame and cropped to a uniform resolution of 1500x1500 pixels. IHC images
282 were further analyzed using Color Selection and Magic Wand tools where areas containing
283 brown staining were manually selected and cut into a separate layer. All images were exported
284 into JPEG format. For staining percentages, quantification was performed using ImageJ.
285 Images were converted from RGB Color into 8-bit grayscale and made Binary to set an
286 automated threshold. Area was then calculated with the Analyze Particles function. Circularity of
287 staining was assessed using the Circularity parameter set to 0.9-1.0.

288

289 **Quantification of lavage cytokines by ELISA.** Immulux 4HBx plates (ThermoFisher Scientific,
290 #3855) were coated with IL-6 capture antibody (ThermoFisher Scientific, MP5-20F3) and left
291 overnight at 4°C. Wells were washed five times with PBS+0.05% Tween 20 and blocked with
292 PBS+5% dry milk solution (Bio-Rad, 1706404) for 1 hour at room temperature. 50µL of lavage
293 sample or standard (R&D systems, 406-ML-005/CF) was added to the blocked wells for 2 hours
294 at room temperature. Bound cytokine was detected using a biotinylated IL-6 detection antibody
295 (ThermoFisher Scientific, MP5-32C11), streptavidin horseradish peroxidase (strep-HRP), and
296 tetramethylbenzidine (TMB) (ThermoFisher Scientific, 34028). Wells were washed three times
297 following the addition of detection antibody and strep-HRP. Reactions were stopped with 2N
298 H_2SO_4 and ODs were read at 450nm. Cytokine concentrations for each sample were determined

299 by plotting OD values on a standard curve using IL-6 recombinant protein. All testing was
300 performed in triplicate.

301

302 **Statistical Analyses.** Two-way mixed effects (ME) models were used to assess % weight loss,
303 and core temperatures (^{o}C) across the factors: i) placebo vs olcegepant protection and ii) dpi.
304 Two-way ME models were also used to assess: i) viral infection vs pretest and ii) placebo vs
305 olcegepant protection for tail vasodilation responses at 3 dpi. Bonferroni multiple comparisons
306 test was the preferred post-hoc analysis method. X-intercept analyses of head recovery (mins)
307 were conducted assuming a quadratic model, least squares regression fitting, and constraints
308 where the x-intercept must be greater than x = 20 mins and the curve fit was approximated to x
309 = 50 mins. Nested 1-way ANOVAs with Tukey post hoc was used to analyze BAL IL-6
310 concentrations and H&E staining (positive SARS-CoV-2 cells per mm^2).

311

312

313 **Conflict of interest statement:** The authors declare no competing financial interests.

314

315 **Acknowledgments**: This research is supported by a COVID-19 research supplement to NIH
316 R01 DC017261 (to AEL with sub-contract to HAC). We would also like to thank Dr. Ralph S.
317 Baric (UNC) for the MA-10 SARS CoV-2 virus stock, the BSL3 facility and staff in the Center
318 for Advanced Research Technologies at the University of Rochester, and the A-BSL3 facility
319 and staff at Cornell University. We would also like to thank Shruti Aryal for assisting with data
320 analysis.

321

322

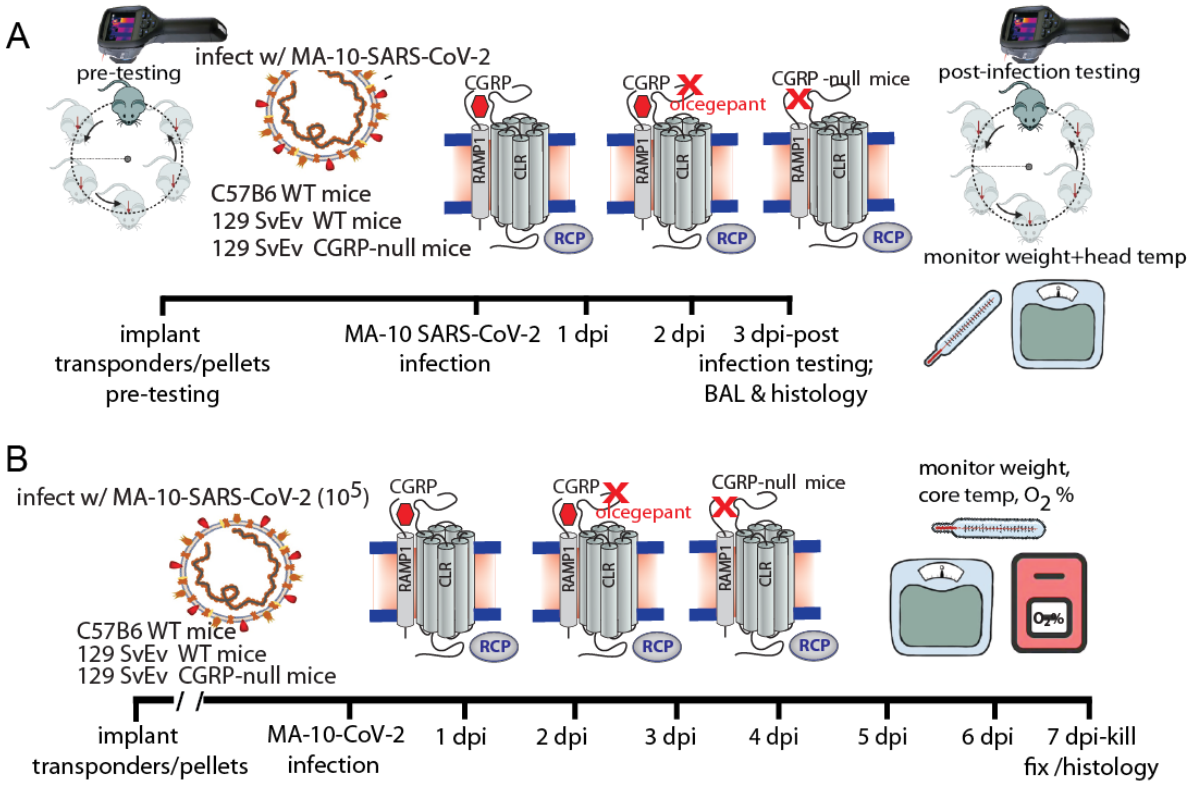

323

324

325 **Fig. 1.** The study timelines are depicted. **A.** WT mice were infected with 10^5 pfu of MA-10
326 SARS-CoV-2 in the presence of placebo or CGRP-receptor antagonist olcegepant slow-release
327 pellets (olcegepant, BIBN4096, Tocris; 2 mg/kg/day/SQ) or mice lacking CGRP were infected
328 with the same virus; animals were then assessed for motion-induced nausea (dizziness) at 3
329 days after viral infection (dpi). At the completion of the nausea testing at 3dpi, bronchoalveolar
330 lavage (BAL) samples were collected for ELISA and lung tissue was obtained from control and
331 virus-infected animals at 3 dpi. Nausea (dizziness) was assessed for 45 minutes when mouse
332 was subjected to an orbital motion, noting temperature profiles (head and tail). **B.** WT mice
333 were infected with 10^5 pfu of MA-10 SARS-CoV-2 in the presence of placebo or CGRP-receptor
334 antagonist olcegepant slow-release pellets (olcegepant, BIBN4096, Tocris; 2 mg/kg/day/SQ) or
335 mice lacking CGRP were infected with the same virus; animals were then monitored for
336 changed in weight, core temperature and oxygen (O_2) saturation from 0 to 7 dpi.

337

338

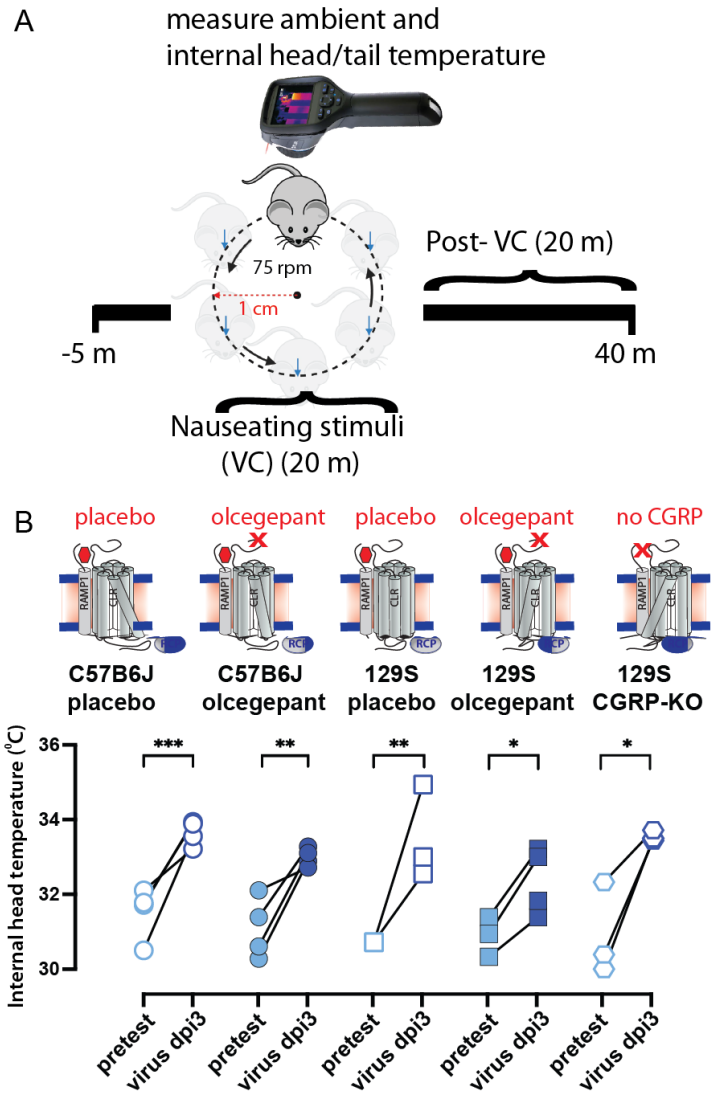

Fig. 2. As shown in the **Fig 1A** timeline, older C57B/6, 129SvEv, and 129 mice lacking CGRP were assessed for nausea (dizziness) when subjected to an orbital rotation, noting temperature profiles (head and tail). **A.** Head and tail temperatures of mice were measured for a total 45 minutes using a FLIR E60 IR camera (model: E64501). This camera was connected to a tripod and positioned approximately 43 cm above an open, plexiglass box (mouse box) used to house an individual mouse during testing. Both the tripod and mouse box are securely attached to the shaker's base. Briefly, baseline measurements were recorded for five minutes prior to the provocative motion (-5 to 0 mins). The provocative motion was an orbital rotation (75 rpm, 2-cm orbital displacement), and mice were recorded for 20 minutes (0 to 20 mins). After 20 minutes, the provocative motion was turned off, and mice were recorded for an additional 20 minutes to measure recovery to baseline (20 to 40 mins). Three mouse strains were tested: C57/B6J WT, 129S WT, and 129S αCGRP-null mice. Within each wild type (WT) strain, four groups of mice

were tested: placebo only, olcegepant only, placebo with 10^5 MA-SARS-CoV-2, and olcegepant with 10^5 SARS-CoV-2 MA-10. Virus-infected mice were tested at Cornell University's ABSL-3 environment, with all pre-infection testing performed at University of Rochester. **B.** All tested mice experienced a fever-like state 3 days post-viral infection (3 dpi). Olcegepant did not have a protective effect in reducing this acute fever-like state at 3 dpi. Significance is listed as *= $p < 0.05$, ** =$p < 0.01$, ***= $p < 0.001$.

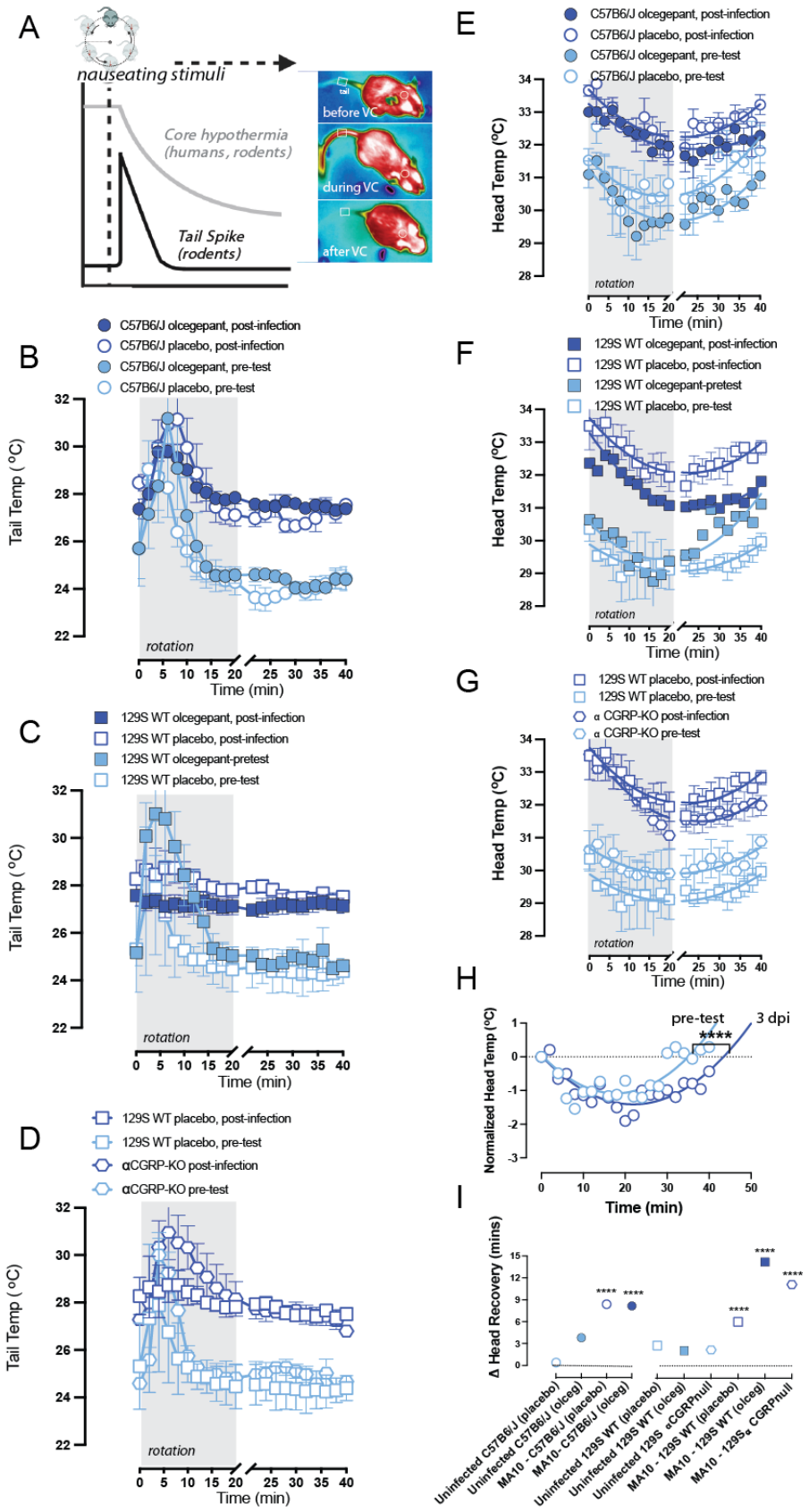
A
nauseating stimuli
Core hypothermia
(humans, rodents)
Tail Spike
(rodents)
tail
before VC
during VC
after VC
B
C57B6/J olcegepant, post-infection
C57B6/J placebo, post-infection
C57B6/J olcegepant, pre-test
C57B6/J placebo, pre-test
Tail Temp (°C)
rotation
Time (min)
C
129S WT olcegepant, post-infection
129S WT placebo, post-infection
129S WT olcegepant-pretest
129S WT placebo, pre-test
Tail Temp (°C)
rotation
Time (min)
D
129S WT placebo, post-infection
129S WT placebo, pre-test
αCGRP-KO post-infection
αCGRP-KO pre-test
Tail Temp (°C)
rotation
Time (min)
E
C57B6/J olcegepant, post-infection
C57B6/J placebo, post-infection
C57B6/J olcegepant, pre-test
C57B6/J placebo, pre-test
Head Temp (°C)
rotation
Time (min)
F
129S WT olcegepant, post-infection
129S WT placebo, post-infection
129S WT olcegepant-pretest
129S WT placebo, pre-test
Head Temp (°C)
rotation
Time (min)
G
129S WT placebo, post-infection
129S WT placebo, pre-test
α CGRP-KO post-infection
α CGRP-KO pre-test
Head Temp (°C)
rotation
Time (min)
H
pre-test
3 dpi
****
Normalized Head Temp (°C)
Time (min)
I
Δ Head Recovery (mins)
****
Uninfected C57B6/J (placebo)
Uninfected C57B6/J (olceg)
MA10 - C57B6/J (placebo)
MA10- C57B6/J (olceg)
Uninfected 129S WT (placebo)
Uninfected 129S WT (olceg)
Uninfected 129S αCGRPnull
MA10 - 129S WT (placebo)
MA10 - 129S WT (olceg)
MA10 - 129Sα CGRPnull

362 **Fig. 3. A.** Upon provocative motion, humans and mice will show a drop in head temperature
363 that recovers once rotation is ceased, and mice show a transient tail spike ~10 min into rotation.
364 When nausea or dizziness is present, the head temperature drop takes longer to recover, and
365 the transient tail spike diminishes or disappears. **B,C,D.** Viral infection diminishes tail
366 vasodilatations and impairs a mouse's natural response to the provocative motion. At time t = 0,
367 mice experience a 20-minute provocative motion and exhibit a significant increase in tail
368 temperature. Δ tails are computed and are corrected for ambient temperature. Findings suggest
369 that olcegepant did not protect against virus-induced changes in tail vasodilation at 3 dpi in all of
370 the strains tested. **E,F,G.** Viral infection impacts recovery from hypothermia after provocative
371 motion. **H.** Second order curve fits observed recovery of head temperatures after provocative
372 motion to baseline. Across all strains, infected mice experienced delayed temperature recovery
373 compared to pretest, with longer recovery profiles (**** = $p < 0.0001$). **I.** No protective effects
374 were seen by olcegepant in temperature recovery for any of the tested strains.

375

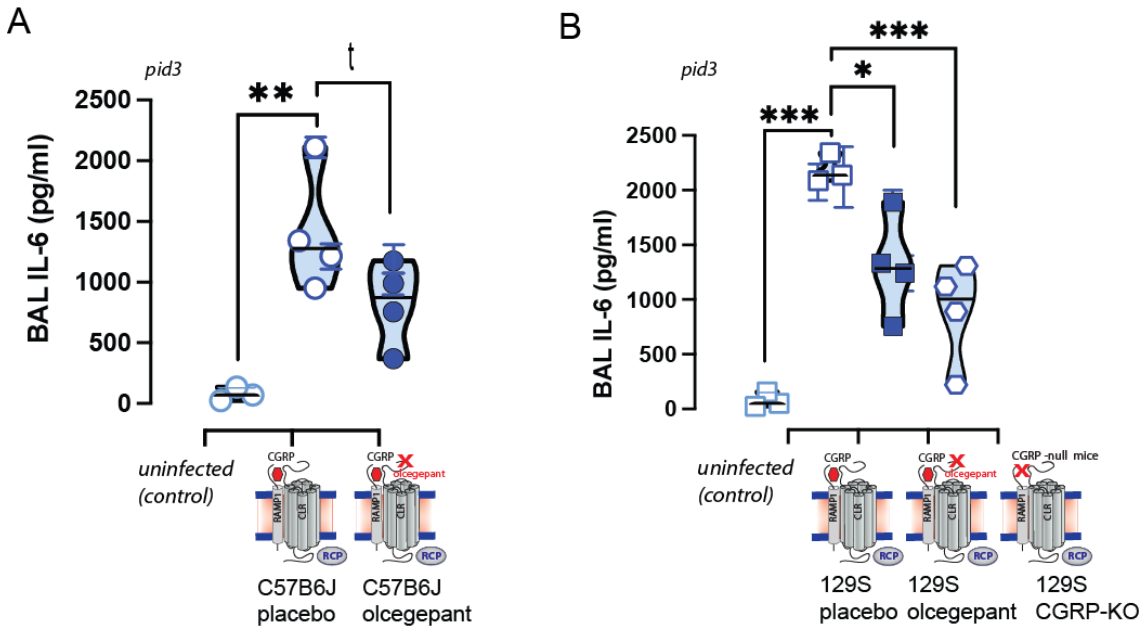

Fig. 4. Bronco-alveolar lavage (BAL) samples were obtained for ELISA testing, and lungs were obtained for subsequent immunohistochemistry at 3 dpi and were analyzed with nested 1-way ANOVAs. MA-SARS-CoV-2 infection increased the release of the inflammatory cytokine IL-6, and this IL-6 release was attenuated by CGRP signaling blockade. In both C57B6/J **(A)** and 129S mice **(B)** strains, IL-6 release was attenuated by olcegepant SQ release. Moreover, in αCGRP null mice, IL-6 cytokine release was statistically equivalent to infected controls given olcegepant and uninfected controls. Significance is listed as *= $p < 0.05$, ** =$p < 0.01$, ***= $p < 0.001$, and the italicized *t* represents a comparison with p-value < 0.1.

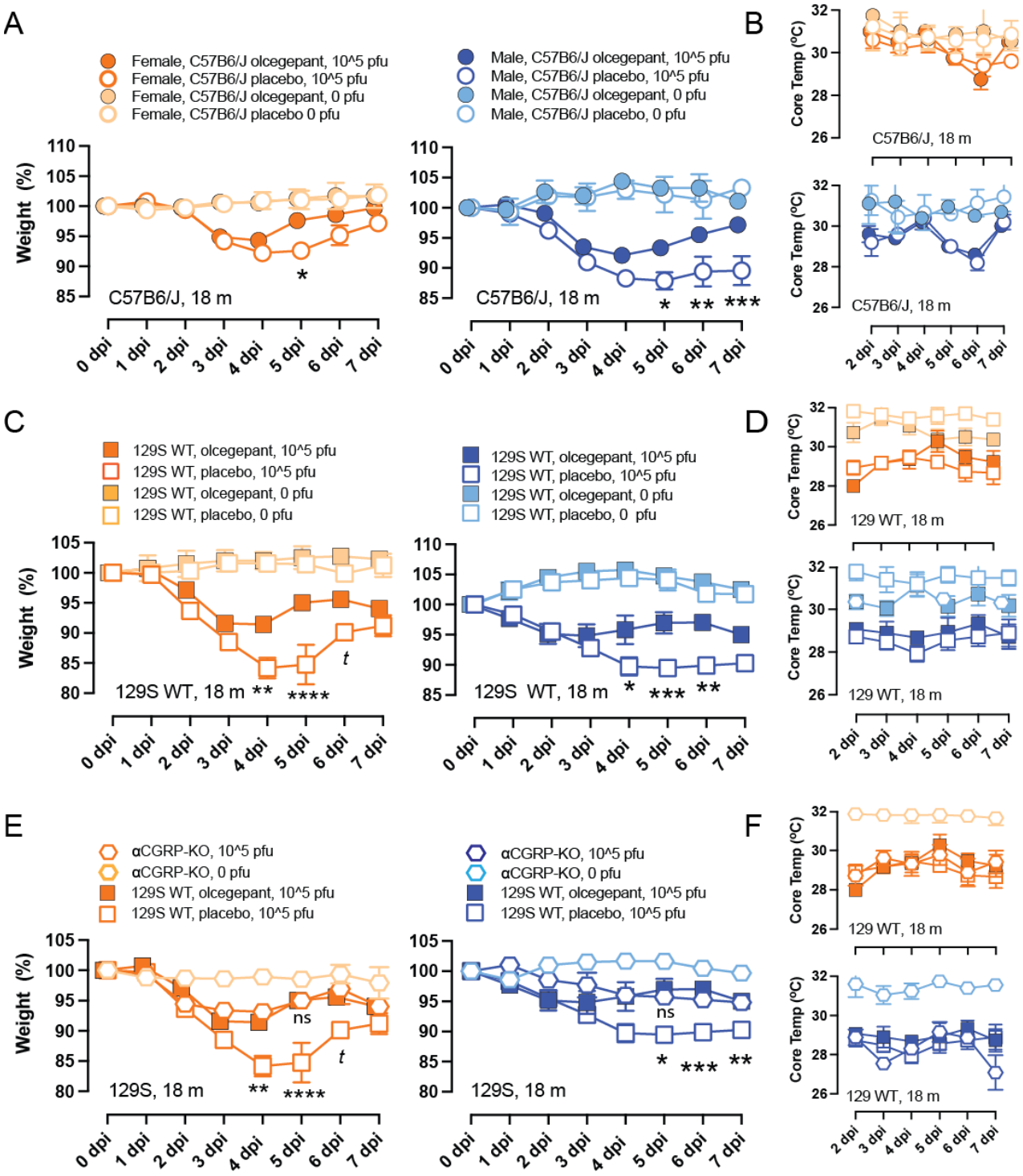

Fig. 5. Older (18 months) female and male mice were tested for weight loss and core temperature drops after infection with MA-10 SARS-CoV-2, 10^5 pfu virus at 0-7 dpi using two-way mixed-effects models and Bonferroni multiple comparisons test. At each dpi, asterisks correspond to comparisons between placebos versus olcegepant in infected mice, since no differences were observed due to olcegepant in uninfected controls **A. C.** We found that animals treated with olcegepant recovered from the initial weight loss, with male mice showing

394 increased protection. **A.** C57B6/J; **C.** 129S. **E.** Similar to the IL-6 findings (**Fig. 4**), mice lacking
395 the CGRP peptide were not significantly different from uninfected controls. **B, D, F.** Viral
396 infection caused detected core temperatures of mice to decrease, and this effect was unaltered
397 by olcegepant treatment. P-values: *= $p < 0.05$, ** =$p < 0.01$, ***= $p < 0.001$, and *t* represents a
398 comparison with p-value < 0.1.
399
400
401

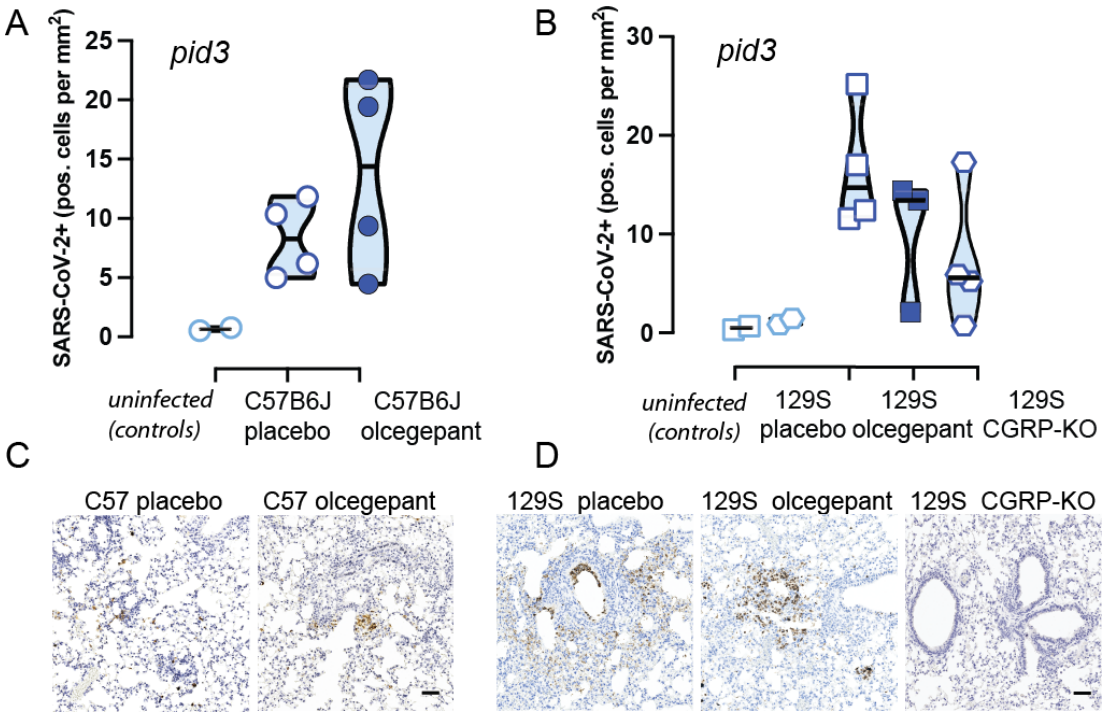

Fig. 6. A&B. There was no statistically significant difference in the number of SARS-CoV-2 antigen-positive cells in the lungs of (**A, C**) C57BL/6J or (**B, D**) 129S mice, between mice that received placebo versus olcegepant pellets at 3 dpi. **C, D.** Representative SARS-CoV-2 immunostaining is shown for 3 dpi lung issues from C57B6/J (**C**), and 129S (**D**) mice. Scale bar is 100 μm.

419 **References:**

420 1. Zhu N, Zhang D, Wang W, Li X, Yang B, Song J, Zhao X, Huang B, Shi W, Lu R, Niu P,
421 Zhan F, Ma X, Wang D, Xu W, Wu G, Gao GF, Tan W, China Novel Coronavirus I,
422 Research T. 2020. A Novel Coronavirus from Patients with Pneumonia in China, 2019. N
423 Engl J Med 382:727-733.

424 2. Bohn MK, Hall A, Sepiashvili L, Jung B, Steele S, Adeli K. 2020. Pathophysiology of
425 COVID-19: Mechanisms Underlying Disease Severity and Progression. Physiology
426 (Bethesda) 35:288-301.

427 3. Saniasiaya J, Kulasegarah J. 2021. Dizziness and COVID-19. Ear Nose Throat J
428 100:29-30.

429 4. Doyle MF. 2022. Central nervous system outcomes of COVID-19. Transl Res 241:41-51.

430 5. Bolay H, Karadas O, Ozturk B, Sonkaya R, Tasdelen B, Bulut TDS, Gulbahar O, Ozge
431 A, Baykan B. 2021. HMGB1, NLRP3, IL-6 and ACE2 levels are elevated in COVID-19
432 with headache: a window to the infection-related headache mechanism. J Headache
433 Pain 22:94.

434 6. Goadsby PJ, Lipton RB, Ferrari MD. 2002. Migraine--current understanding and
435 treatment. N Engl J Med 346:257-70.

436 7. Lassen LH, Haderslev PA, Jacobsen VB, Iversen HK, Sperling B, Olesen J. 2002.
437 CGRP may play a causative role in migraine. Cephalalgia 22:54-61.

438 8. Tringali G, Navarra P. 2019. Anti-CGRP and anti-CGRP receptor monoclonal antibodies
439 as antimigraine agents. Potential differences in safety profile postulated on a
440 pathophysiological basis. Peptides 116:16-21.

441 9. Scuteri D, Adornetto A, Rombola L, Naturale MD, Morrone LA, Bagetta G, Tonin P,
442 Corasaniti MT. 2019. New Trends in Migraine Pharmacology: Targeting Calcitonin
443 Gene-Related Peptide (CGRP) With Monoclonal Antibodies. Front Pharmacol 10:363.

444 10. Robertson CE. 2020. Could CGRP antagonists be helpful in the fight against COVID-19?
445 Headache doi:10.1111/head.13853.

446 11. Assas BM, Miyan JA, Pennock JL. 2014. Cross-talk between neural and immune
447 receptors provides a potential mechanism of homeostatic regulation in the gut mucosa.
448 Mucosal Immunol 7:1283-9.

449 12. Assas BM, Pennock JI, Miyan JA. 2014. Calcitonin gene-related peptide is a key
450 neurotransmitter in the neuro-immune axis. Front Neurosci 8:23.

451 13. Channappanavar R, Perlman S. 2017. Pathogenic human coronavirus infections: causes
452 and consequences of cytokine storm and immunopathology. Semin Immunopathol
453 39:529-539.

454 14. Aghagoli G, Gallo Marin B, Katchur NJ, Chaves-Sell F, Asaad WF, Murphy SA. 2021.
455 Neurological Involvement in COVID-19 and Potential Mechanisms: A Review. Neurocrit
456 Care 34:1062-1071.

457 15. Liu Y, Zhang C, Huang F, Yang Y, Wang F, Yuan J, Zhang Z, Qin Y, Li X, Zhao D, Li S,
458 Tan S, Wang Z, Li J, Shen C, Li J, Peng L, Wu W, Cao M, Xing L, Xu Z, Chen L, Zhou
459 C, Liu WJ, Liu L, Jiang C. 2020. Elevated plasma levels of selective cytokines in COVID-
460 19 patients reflect viral load and lung injury. Natl Sci Rev 7:1003-1011.

461 16. Carpenter KC, Yang J, Xu JJ. 2023. Animal Models for the Study of Neurologic
462 Manifestations Of COVID-19. Comp Med 73:91-103.

463 17. Kuba K, Imai Y, Rao S, Gao H, Guo F, Guan B, Huan Y, Yang P, Zhang Y, Deng W,
464 Bao L, Zhang B, Liu G, Wang Z, Chappell M, Liu Y, Zheng D, Leibbrandt A, Wada T,
465 Slutsky AS, Liu D, Qin C, Jiang C, Penninger JM. 2005. A crucial role of angiotensin
466 converting enzyme 2 (ACE2) in SARS coronavirus-induced lung injury. Nat Med 11:875-
467 9.

468 18. Ziegler CGK, Allon SJ, Nyquist SK, Mbano IM, Miao VN, Tzouanas CN, Cao Y, Yousif
469 AS, Bals J, Hauser BM, Feldman J, Muus C, Wadsworth MH, 2nd, Kazer SW, Hughes
470 TK, Doran B, Gatter GJ, Vukovic M, Taliaferro F, Mead BE, Guo Z, Wang JP, Gras D,
471 Plaisant M, Ansari M, Angelidis I, Adler H, Sucre JMS, Taylor CJ, Lin B, Waghray A,
472 Mitsialis V, Dwyer DF, Buchheit KM, Boyce JA, Barrett NA, Laidlaw TM, Carroll SL,
473 Colonna L, Tkachev V, Peterson CW, Yu A, Zheng HB, Gideon HP, Winchell CG, Lin
474 PL, Bingle CD, Snapper SB, Kropski JA, Theis FJ, et al. 2020. SARS-CoV-2 Receptor
475 ACE2 Is an Interferon-Stimulated Gene in Human Airway Epithelial Cells and Is
476 Detected in Specific Cell Subsets across Tissues. Cell doi:10.1016/j.cell.2020.04.035.

477 19. Dinnon KH, 3rd, Leist SR, Schafer A, Edwards CE, Martinez DR, Montgomery SA, West
478 A, Yount BL, Jr., Hou YJ, Adams LE, Gully KL, Brown AJ, Huang E, Bryant MD, Choong
479 IC, Glenn JS, Gralinski LE, Sheahan TP, Baric RS. 2020. A mouse-adapted model of
480 SARS-CoV-2 to test COVID-19 countermeasures. Nature 586:560-566.

481 20. Dinnon KH, 3rd, Leist SR, Schafer A, Edwards CE, Martinez DR, Montgomery SA, West
482 A, Yount BL, Jr., Hou YJ, Adams LE, Gully KL, Brown AJ, Huang E, Bryant MD, Choong
483 IC, Glenn JS, Gralinski LE, Sheahan TP, Baric RS. 2021. Publisher Correction: A
484 mouse-adapted model of SARS-CoV-2 to test COVID-19 countermeasures. Nature
485 590:E22.

486 21. Shafaqat MR, Anne EL. 2023. Calcitonin Gene-Related Peptide (CGRP) Receptor
487 Antagonism Reduces Motion Sickness Indicators in Mouse Migraine Models. bioRxiv
488 doi:10.1101/2022.06.03.494762:2022.06.03.494762.

489 22. Tu L, Poppi L, Rudd J, Cresswell ET, Smith DW, Brichta A, Nalivaiko E. 2017. Alpha-9
490 nicotinic acetylcholine receptors mediate hypothermic responses elicited by provocative
491 motion in mice. Physiol Behav 174:114-119.

492 23. Del Vecchio F, Nalivaiko E, Cerri M, Luppi M, Amici R. 2014. Provocative motion causes
493 fall in brain temperature and affects sleep in rats. Exp Brain Res 232:2591-9.

494 24. Mazloumi Gavgani A, Hodgson DM, Nalivaiko E. 2017. Effects of visual flow direction on
495 signs and symptoms of cybersickness. PLoS One 12:e0182790.

496 25. Ngampramuan S, Cerri M, Del Vecchio F, Corrigan JJ, Kamphee A, Dragic AS, Rudd
497 JA, Romanovsky AA, Nalivaiko E. 2014. Thermoregulatory correlates of nausea in rats
498 and musk shrews. Oncotarget 5:1565-75.

499 26. Romano F, Caramia N, Straumann D, Nalivaiko E, Bertolini G. 2017. Cross-coupling
500 vestibular stimulation: motion sickness and the vestibulo-sympathetic reflex. J Neurol
501 doi:10.1007/s00415-017-8496-x.

502 27. Doods H, Hallermayer G, Wu D, Entzeroth M, Rudolf K, Engel W, Eberlein W. 2000.
503 Pharmacological profile of BIBN4096BS, the first selective small molecule CGRP
504 antagonist. Br J Pharmacol 129:420-3.

505 28. Mallee JJ, Salvatore CA, LeBourdelles B, Oliver KR, Longmore J, Koblan KS, Kane SA.
506 2002. Receptor activity-modifying protein 1 determines the species selectivity of non-
507 peptide CGRP receptor antagonists. J Biol Chem 277:14294-8.

508 29. Han D. 2019. Association of Serum Levels of Calcitonin Gene-related Peptide and
509 Cytokines during Migraine Attacks. Ann Indian Acad Neurol 22:277-281.

510 30. Aedo-Sanchez C, Gutierrez G, Aguilar-Vidal E. 2023. COVID-19 and Vestibular
511 Symptoms and Assessment: A Review. Audiol Neurootol doi:10.1159/000533448:1-7.

512 31. Jeong M, Ocwieja KE, Han D, Wackym PA, Zhang Y, Brown A, Moncada C, Vambutas
513 A, Kanne T, Crain R, Siegel N, Leger V, Santos F, Welling DB, Gehrke L, Stankovic KM.
514 2021. Direct SARS-CoV-2 infection of the human inner ear may underlie COVID-19-
515 associated audiovestibular dysfunction. Commun Med (Lond) 1:44.

516 32. Abobaker A, Darrat M. 2021. Letter to the Editor From Abobaker and Darrat: "Circulating
517 Levels of Calcitonin Gene-Related Peptide Are Lower in COVID-19 Patients". J Endocr
518 Soc 5:bvab052.

519 33. Ochoa-Callejero L, Garcia-Sanmartin J, Villoslada-Blanco P, Iniguez M, Perez-Matute P,
520 Pujadas E, Brody R, Oteo JA, Martinez A. 2021. Response to Letter to the Editor from
521 Abobaker and Darrat: "Circulating levels of Calcitonin Gene-Related Peptide Are Lower
522 in COVID-19 Patients". J Endocr Soc 5:bvab053.

523 34. Rizzi M, Tonello S, Morani F, Rizzi E, Casciaro GF, Matino E, Costanzo M, Zecca E,
524 Croce A, Pedrinelli A, Vassia V, Landi R, Mallela VR, D'Onghia D, Minisini R, Bellan M,
525 Castello LM, Gavelli F, Avanzi GC, Patrucco F, Pirisi M, Colangelo D, Sainaghi PP.
526 2022. CGRP Plasma Levels Correlate with the Clinical Evolution and Prognosis of
527 Hospitalized Acute COVID-19 Patients. Viruses 14.

528 35. Fan C, Wu Y, Rui X, Yang Y, Ling C, Liu S, Liu S, Wang Y. 2022. Animal models for
529 COVID-19: advances, gaps and perspectives. Signal Transduct Target Ther 7:220.

530 36. Choi S, Lee J, Kim S, Lee YW, Kim GC, Hong SM, An SH, Noh H, Kim KE, On D, Lee
531 SG, Jang HJ, Kim SH, Kim J, Seo JS, Kim JJ, Park IH, Oh J, Kim DJ, Yoon JH, Seok
532 SH, Lee YJ, Kim SY, Kim YB, Hwang JY, Lee HJ, Kim HB, Park JW, Yun JW, Shin JS,
533 Seo JY, Nam KT, Choi KS, Kwon HK, Lee HY, Kim JK, Seong JK. 2023. A longitudinal
534 molecular and cellular lung atlas of lethal SARS-CoV-2 infection in K18-hACE2
535 transgenic mice. EBioMedicine 99:104932.

536 37. Caronna E, Jose Gallardo V, Alpuente A, Torres-Ferrus M, Sanchez-Mateo NM,
537 Viguera-Romero J, Lopez-Veloso AC, Lopez-Bravo A, Gago-Veiga AB, Irimia Sieira P,
538 Porta-Etessam J, Santos-Lasaosa S, Pozo-Rosich P, Spanish C-CSG. 2021. Safety of
539 anti-CGRP monoclonal antibodies in patients with migraine during the COVID-19
540 pandemic: Present and future implications. Neurologia (Engl Ed) 36:611-617.

38. Grassini A, Marcinno A, Roveta F, Gallo E, Cermelli A, Boschi S, Rubino E, Rainero I. 2021. Impact of COVID-19 on chronic migraine treated with erenumab: a case report. Neurol Sci 42:3079-3081.

39. Ozkan E, Celebi O, Keskin O, Gursoy A, Gursoy-Ozdemir Y. 2022. Is Persistent Post-COVID Headache Associated With Protein-Protein Interactions Between Antibodies Against Viral Spike Protein and CGRP Receptor?: A Case Report. Front Pain Res (Lausanne) 3:858709.

40. Littlefield KM, Watson RO, Schneider JM, Neff CP, Yamada E, Zhang M, Campbell TB, Falta MT, Jolley SE, Fontenot AP, Palmer BE. 2022. SARS-CoV-2-specific T cells associate with inflammation and reduced lung function in pulmonary post-acute sequalae of SARS-CoV-2. PLoS Pathog 18:e1010359.

41. Dinnon KH, Leist SR, Okuda K, Dang H, Fritch EJ, Gully KL, De la Cruz G, Evangelista MD, Asakura T, Gilmore RC, Hawkins P, Nakano S, West A, Schafer A, Gralinski LE, Everman JL, Sajuthi SP, Zweigart MR, Dong S, McBride J, Cooley MR, Hines JB, Love MK, Groshong SD, VanSchoiack A, Phelan SJ, Liang Y, Hether T, Leon M, Zumwalt RE, Barton LM, Duval EJ, Mukhopadhyay S, Stroberg E, Borczuk A, Thorne LB, Sakthivel MK, Lee YZ, Hagood JS, Mock JR, Seibold MA, O'Neal WK, Montgomery SA, Boucher RC, Baric RS. 2022. A model of persistent post SARS-CoV-2 induced lung disease for target identification and testing of therapeutic strategies. bioRxiv doi:10.1101/2022.02.15.480515.

42. Jansen EB, Orvold SN, Swan CL, Yourkowski A, Thivierge BM, Francis ME, Ge A, Rioux M, Darbellay J, Howland JG, Kelvin AA. 2022. After the virus has cleared-Can preclinical models be employed for Long COVID research? PLoS Pathog 18:e1010741.

43. Shapira T, Monreal IA, Dion SP, Buchholz DW, Imbiakha B, Olmstead AD, Jager M, Desilets A, Gao G, Martins M, Vandal T, Thompson CAH, Chin A, Rees WD, Steiner T, Nabi IR, Marsault E, Sahler J, Diel DG, Van de Walle GR, August A, Whittaker GR, Boudreault PL, Leduc R, Aguilar HC, Jean F. 2022. A TMPRSS2 inhibitor acts as a pan-SARS-CoV-2 prophylactic and therapeutic. Nature 605:340-348.

44. Achanta R, Shaji A, Smith K, Lucchi A, Fua P, Susstrunk S. 2012. SLIC superpixels compared to state-of-the-art superpixel methods. IEEE Trans Pattern Anal Mach Intell 34:2274-82.

45. Bankhead P, Loughrey MB, Fernandez JA, Dombrowski Y, McArt DG, Dunne PD, McQuaid S, Gray RT, Murray LJ, Coleman HG, James JA, Salto-Tellez M, Hamilton PW. 2017. QuPath: Open source software for digital pathology image analysis. Sci Rep 7:16878.

46. Shapira T, Monreal IA, Dion SP, Jager M, Desilets A, Olmstead AD, Vandal T, Buchholz DW, Imbiakha B, Gao G, Chin A, Rees WD, Steiner T, Nabi IR, Marsault E, Sahler J, August A, Van de Walle G, Whittaker GR, Boudreault PL, Aguilar HC, Leduc R, Jean F. 2021. A novel highly potent inhibitor of TMPRSS2-like proteases blocks SARS-CoV-2 variants of concern and is broadly protective against infection and mortality in mice. bioRxiv doi:10.1101/2021.05.03.442520.